SMiRT-12 / K. Kussmaul (Editor)

STUDY ON STRENGTH OF THICK REINFORCED CONCRETE SLAB WITH OPENING - PART 1: OUTLINE OF STUDY AND SCALE MODEL TESTS

T. Hirai[1], M. Itoh[1], T. Nishikawa[1], K. Takei[1], T. Kanazu[2], K. Ujiie[3] and H. Mizuuchi[3], S. Tsurumaki[3]

[1]Electric Power Development Company, Ltd., [2]Central Research Institute of the Electric Power Industry, [3]Kobori Research Complex, Inc.

Abstract

This study focussed on the support structure of the reactor in a demonstration plant of an advanced thermal reactor (ATR). In order to verify the structural soundness of the thick reinforced concrete slab under out-of-plane force, we employed two types of reduced scale models. We performed experiments in which we gradually increased vertical load, and carried out a non-linear finite element analysis (FEA) . As a result, we were able to evaluate the strength of the support slab of the reactor was of the flexural failure type, and that the slab had adequate strength. Furthermore, we were able to verify the safety of the support slab, taking the ultimate bending strength of the support slab to be the sum of the strength of its short span cantilever beams. In addition, using non-linear FEA on layered shell elements, we were able to ascertain the failure process, and confirm suitability for practical applications.

1. Introduction

The type of advanced thermal reactor (ATR) which is being designed in Japan today is demonstration plant, of the heavy water moderated boiling light water cooled pressure-tube type. The reactor core is supported by a reinforced concrete slab spanning 14.0 m x 19.6 m, known as the support slab. There is an 8.576 m diameter circular opening at the center of the slab, where pressure tubes pass vertically through the reactor. This arrangement is further supported by surrounding walls. The structure of the support slab is outlined in Fig. 1. The thickness of the support slab is 1.7 m thick around the opening, all the way to the edge of the short axis. The thickness of the slab increases in steps. At the center of the long axis the slab is 2.0 m thick, and at the edges increases to 3.0 m. The intersection of the support slab and the lower wall is shown as the haunched portion in the figure.

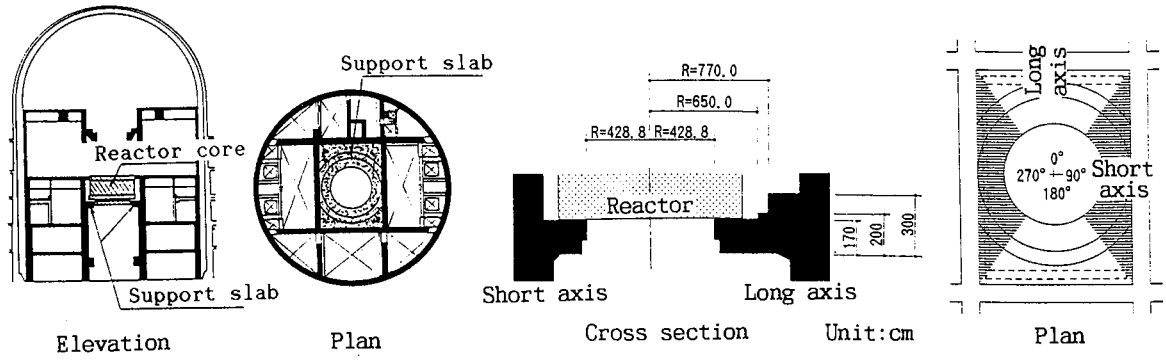

Fig.1 Outline of the support slab

The reactor core is designed to be inserted into the opening of the support slab, and has a weight of 25.7 MN. Out-of-plane force is transferred to the support slab via sole plates, installed in 24 places at 15 degree angles around the opening of the support slab. During normal operation, the load which is applied to the support slab by the reactor core is only live load in the vertical direction. However, because the support slab is rectangularly shaped, the load which comes to bear on each of the 24 locations of the sole plates is not uniform, as it depends on the relative rigidity of the support slab compared to the reactor core. As can be seen in hatched portion of Fig. 1, the short dimension of the slab supports nearly 70% of the reactor core's weight. Therefore, the structural soundness of the support slab depends to a large extent on the strength and failure mode of its short axis.

To confirm the ultimate failure mode of the support slab, it is important to consider both failure process and ultimate strength in the design of the support slab. However, at present there is no way to accurately calculate the ultimate strength of a reinforced concrete slab which has an opening in the center, especially with respect to out-of-plane force on a thick plate. Therefore, the aim of this study was to focus on the ultimate strength and failure mode of the support slab with respect to out-of-plane force, in an effort to ascertain its structural viability.

2. Research Outline

2.1. Research Plan

A flowchart for the research is shown in Fig. 2. In order to evaluate the structural viability of support slab under out-of-plane force due to gradually increased vertical force loading, we performed two kinds of static loading tests and a simulation analysis using a non-linear FEA.

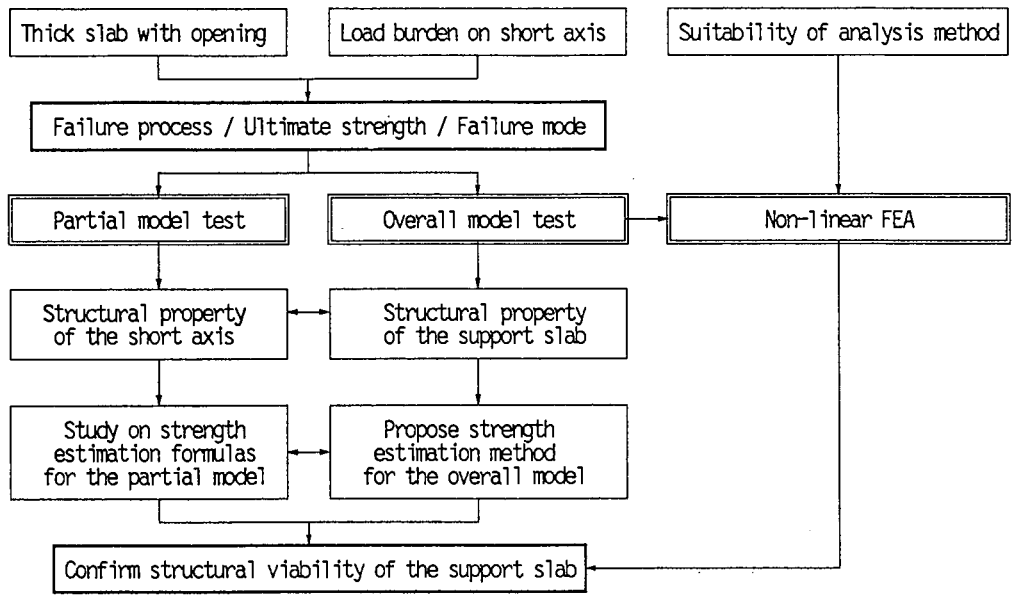

Fig.2 Research flowchart

2.2. Partial Model Test

In order to understand the strength and failure mode of the support slab, in which approximately 70% of the weight of the reactor is applied to the short axis of the slab, we performed a 1/3 scale partial model test. The specimen was a support slab scaled down in identical proportions to unit width, connected to the stiff walls by short span cantilever beams. The conditions of the experiment are shown in Photo 1. Three model specimens were set up as a parameter for the tension rebar ratio and shear span ratio. The basic results of the experiment are shown in Table 1. The shear force bearing on the short span cantilevers is a truss mechanism of shear transfer when the shear span ratio was 0.63, with shear reinforcement tension applied when the shear span ratio was 1.13. It was clear from these results that the failure mode was of the flexural failure type.

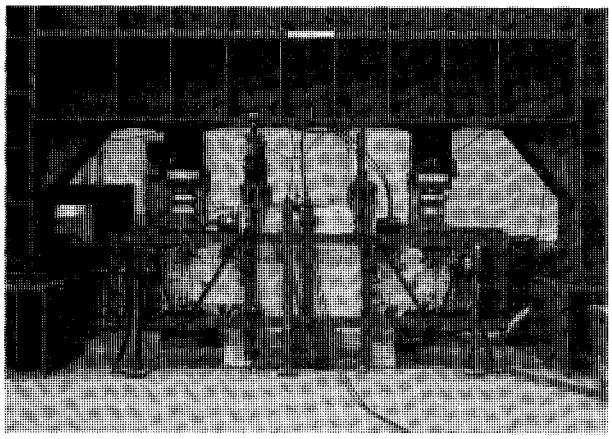

Photo 1 View of the partial model test

Table 1 Basic results of the partial model test

Parameters / Results		Specimen P1	P2	P3
Shear span ratio		0.63	1.13	0.63
Main rebar ratio	(%)	0.70	0.70	0.98
Flexural crack	(MN)	0.20	0.11	0.22
Shear crack	(MN)	0.46	0.36	0.46
Main rebar yield	(MN)	1.18	0.64	1.66
Collapse of concrete	(MN)	1.31	0.71	1.74

2.3. Overall Model Test

Using a 1/5 scale overall model, we attempted to model as faithfully as possible the support slab, installing rigid walls around the specimen. The load was modeled with the distributed loading mode of the reactor in 3 systems, with 12 loading points. The conditions of this experiment are shown in photo 2. The experiment determined that the support slab under out-of-plane force showed no loss of stiffness after rebar yielding in one part, and showed an extremely stable load-displacement relationship up to the load limit of the loading apparatus. Furthermore, compressive stress ring due to out-of-plane force was evident in the area around the opening. The results of this experiment are summarized in Table 2.

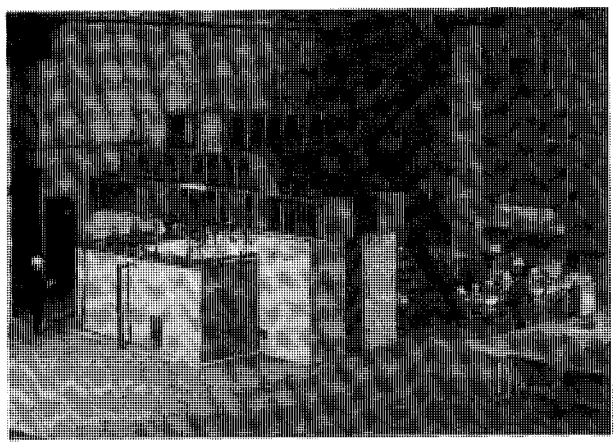

Photo 2 View of the overall model test

Table 2 Basic results of the overall model test

Events (direction)	Total load (MN)
Initial crack (90°)	1.44
Radial crack on the upper surface (90°)	3.49
Circular crack on the lower surface (90°)	5.53
Tension yield of radial rebar (90°)	7.96
Tension yield of radial rebar (60°)	9.60
Compressive yield of circular rebar (90°)	12.24

2.4. Evaluation of Test Results

We examined an application of evaluation formulas used in recent research was adequate for the evaluation method of maximum strength of the partial model. We confirmed that computation methods now in use for ultimate bending strength were appropriate for calculating the ultimate bending strength of the partial model.

In comparing the experimental results from the partial model with those from the overall model, it became clear that the overall model gave the evidence of due to circumferential restricting effect. Therefore, the cracking strength and ultimate strength were larger in the overall model than in the partial model. Furthermore, the strength of the overall model could be estimated conveniently and conservatively as a projected sum of the strengths of the partial models. We expand on the details of this evaluation in Part 2.

2.5. Non-linear Finite Element Analysis

For the overall model test, a non-liner FEA using layered shell elements was performed. This analysis gave a clear picture of failure process of the overall model. It is found that this analytical code is fully appropriate for use in evaluating failure process and the design of reinforced concrete slab with an opening, subjected out-of-plane force.

This is explained in detail in Part 3.

3. Partial Model Test

3.1. Test Method

(1) Specimen

The structure of the specimen is outlined in Fig. 3, and a list of test specimens is presented in Table 3. The basic P1 specimen was a 1/3 scale model, with the short axis of the support slab centered at 90 degrees with 15 degree range. For the P2 specimen we brought the shear span ratio from 0.63 to 1.13, modeled at a 90 +/-30 degree direction. The P3 specimen had a 40% higher rebar quantity than the P1 specimen. All three specimens were of identical shape, with 2 cantilever beams symmetrically connected to rigid walls. The anchor plate system was used on one side as an anchoring method for the rebars, while the bar bend anchor system was used on the other side.

Table 3 List of the partial model specimens

Specimen	Length (cm)	Shear span ratio	Main rebar ratio (%)	Shear rebar ratio (%)	Compressive strength of concrete (MPa)
P1	38.9	0.63	0.70	1.07	32.0
P2	69.8	1.13	0.70	1.07	30.9
P3	38.9	0.63	.0.98	1.07	31.5

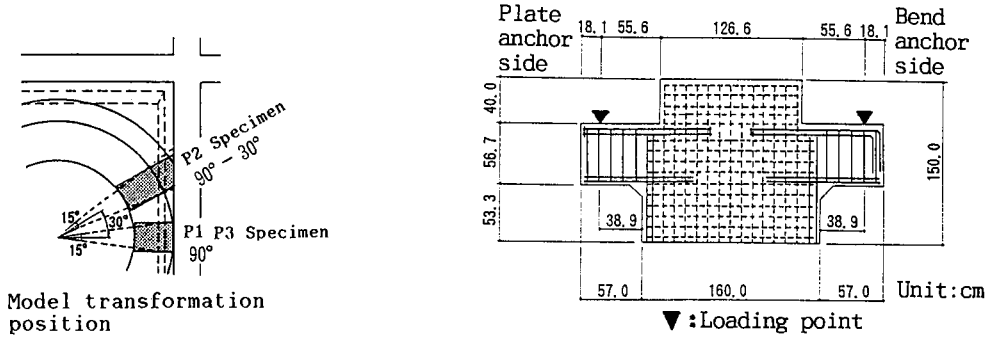

Fig.3 The partial model specimen (P1 Specimen)

(2) Loading Method

The specimen was tightly connected to the reaction floor, enabling an equal vertical force loading in a gradually increased monotonic cycle. Both beams were loaded to the concrete failure. In case one cantilever beam failed before the other, the load on the failed beam was held constant, while the load on the remaining beam was gradually increased. The loading steps are shown in Fig. 4.

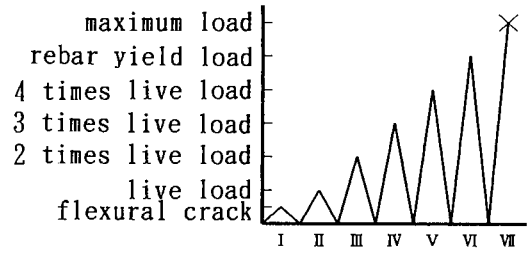

Fig.4 Loading cycle for the partial model test

3.2. Test Results

(1) Failure Process

The failure process for each specimen was as follows: 1) occurrence of flexural cracks, 2) occurrence of shear cracks from the loading points to the haunch, 3) upper rebar yielding due to tension, and 4) collapse of concrete at the haunch. Thus, failure mode of each specimen was flexural failure type.

(2) Vertical Displacement at the Loading Points

The load-displacement relationship of specimen P1 is described in Fig. 5, and expressed in an envelope curve in Fig. 6. In each specimen, until the occurrence of flexural cracks and yield of the upper rebar, stiffness remained constant as deformation progressed, until maximum load was achieved and the concrete failed. Where the shear span ratio was relatively small, in specimens P1 and P3, load dropped suddenly after the concrete failed. In specimen P2, the shear span ratio was comparatively large, but even though we increased the load by as much as 12 times over that of the time of yield displacement, no sudden drop in the load occurred.

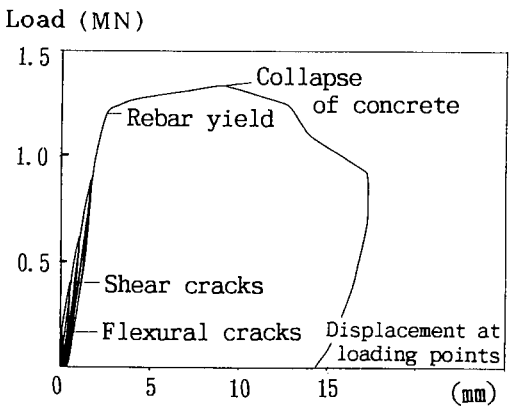

Fig.5 Load-displacement relationship (Plate anchor side of the P1 specimen)

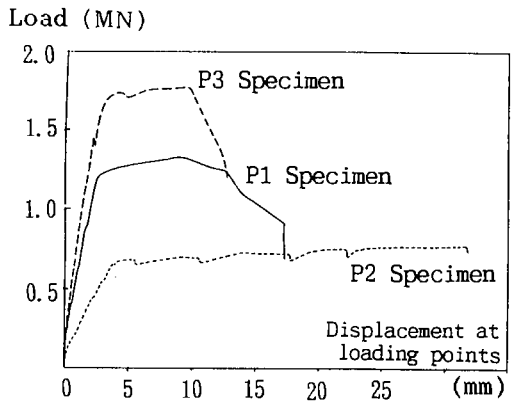

Fig.6 Load-displacement relationship (P1 P2 P3 specimens)

(3) Rebar Strain

Fig. 7 shows the load-rebar strain relationship for each specimen on the rebar with anchor plate system side, expressed on an envelope curve. As also seen in the load-displacement relationship, when flexural cracks occurred, the curve rises slowly. However, after that point the curve climbs almost straight up, as strain reaches yield strain. Although strain was almost absent in the lower bars of specimens P1 and P3, by contrast specimen P2 showed a maximum compressive strain to the degree of 500 x 10(*-6).

(4) Shear Rebar Strain

Fig. 8 shows the load-shear rebar strain relationship for each specimen on the re-bar with anchor plate side, expressed on an envelope curve. Specimens P1 and P3 showed compressive strain in the beginning, which as shear strain progressed, shifted to tensile strain, and after collapse of the concrete, showed a sudden increase leading to yield strain. Even in P2 specimen showed small compressive strain at first, which changed to tensile strain as the load increased, not leading to yield strain.

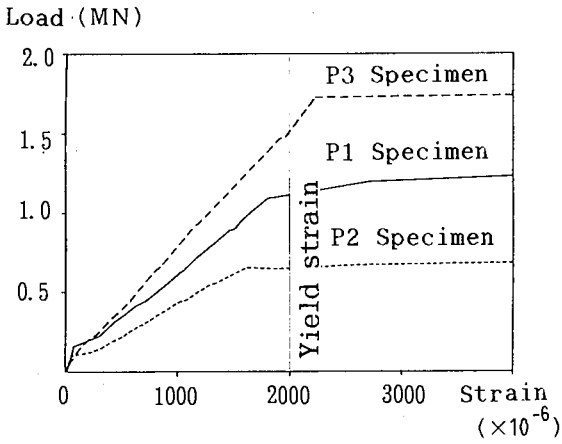

Fig.7 Load-main rebar strain relationship

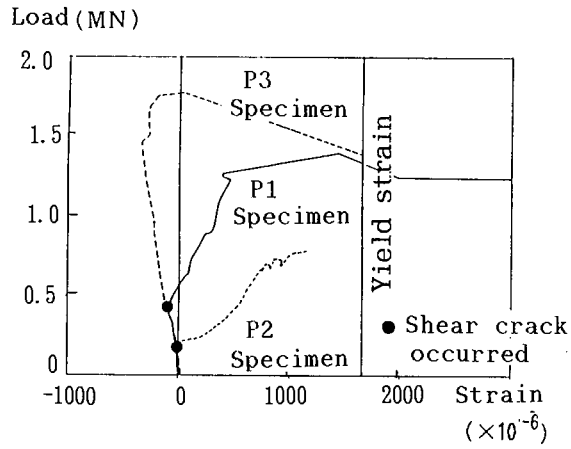

Fig.8 Load-shear rebar strain relationship

(5) Final Condition of the Specimen

Fig. 9 shows the cracking and failure condition of specimen P1 at the time of maximum loading. At 0.20 MN, flexural cracks started to appear slightly on the sides of the upper portion of the specimen. At 0.46 MN, along with progressive development of flexural cracks, shear cracks appeared diagonally from the loading points toward the direction of the haunch. The haunch of the concrete failed at the maximum load strength of 1.31 MN.

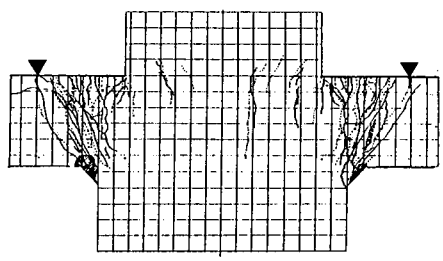

Fig.9 Final condition of the partial model (P1 Specimen)

3.3. Shear Transfer Mechanism of the Partial Model Specimen

In specimen P2, where the shear ratio was relatively large, deformation due to bending was dominant in standard reinforced concrete beams. The experiment also made clear that the tension due to shear force was borne by the shear rebars. On the other hand, for the shear transfer mechanism in specimens P1 and P3, where the shear ratio was small, we conjectured that the concrete compressive struts, from loading points to the haunch and tension rebar consisted of a truss type mechanism (refer to Fig. 10). There was no influence or difference from the anchor method on strength and deformation capacity.

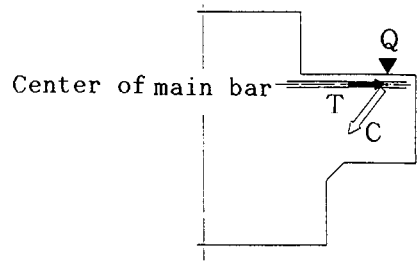

Fig.10 Shear transfer mechanism of P1, P3 specimens

4. Overall Model Test

4.1. Test Method

(1) Specimen

The specimen is shown in Fig. 11. The specimen is a 1/5 scale model, and was modeled as faithfully as possible after the support slab, installing rigid walls around the four sides of the specimen. The specimen was tightly connected to the floor of the laboratory by PC rods. The rebar arrangements were structured as follows: radial rebars of 10 mm diameter arranged radially, circular rebars of 10 mm diameter arranged in concentric circles, and shear reinforcement rebars of 10 mm or 6 mm diameter installed at the intersection of the radial and circular rebars. Through this arrangement we were able to model the rebar ratio designed for the support slab. Yielding stress of the rebar was 407.0 MPa, and the compressive strength of the concrete under sealed condition at the beginning of the experiment was 32.5 MPa.

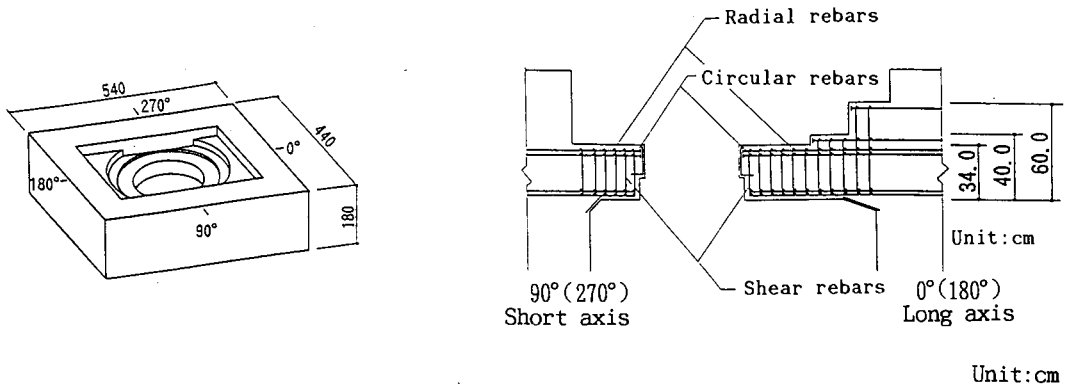

Fig.11 The overall model specimen

(2) Loading Method

Fig. 12 shows the jack arrangement and load ratio. Twelve hydraulic jacks set at angles of 30 degree pitch applied vertical loading around the opening. The reaction force applied by the hydraulic jacks was borne by a loading frame composed of reinforced concrete columns, and steel frame beams. The ratio of loading for each jack was determined by the analytical result, based on the weight of the reactor. In other words, as shown in Fig. 12, application rates were divided into 3 types, A, B, and C. The specimen was loaded gradually in monotonic cycles loading, maintaining a load ratio of A:B:C: = 1.0: 0.7: 0.43. Furthermore, the B type jack reached the limit of the loading capacity at a total load of 10.4 MN. After reaching the limit of the force, the B type jacks were held constant at 0.98 MN. Only the A and C types were had the load increased at the abovementioned load ratio. The experiment ended at the limit of the loading capacity, with a total load of 12.7 MN. The loading steps are shown in Fig. 13.

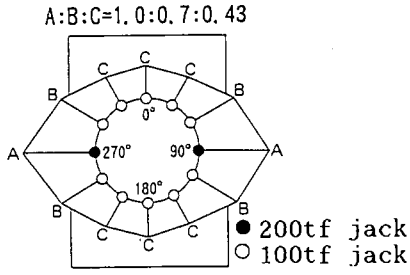

Fig.12 Jack arrangement and load ratio

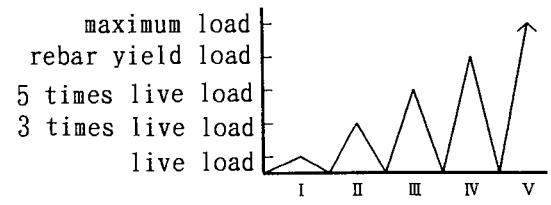

Fig.13 Loading cycle for the overall model test

4.2. Test Results

(1) Failure Process

The failure process is shown in Fig. 14. Failure progressed in the order of the numbers indicated in the Fig. 14, as follows: 1) there was an occurrence of cracks on the upper surface of the slab along the short axis at loading of 1.4 MN, corresponding to 1.4 times the weight of the reactor itself; 2) radial cracks occurred on the lower surface of the slab along the short axis after loading 5.5 MN, corresponding to 5.4 times the weight of the reactor itself; 3) tension yielding was evident radial rebars in the upper part of the slab along the short axis after loading 8.0 MN, corresponding to 7.7 times the weight of the reactor itself; 4) compressive yielding occurred in the circular rebars in the upper part of the slab along the short axis after loading 12.2 MN, corresponding to 12 times the weight of the reactor itself; 5) compressive failure occurred at the haunch along the short axis after loading 12.7 MN, corresponding to 12.5 times the weight of the reactor itself, at which point the experiment was concluded. Occurrence of cracks and yield of rebar progressed from the short to the long axis with the increase in the loading.

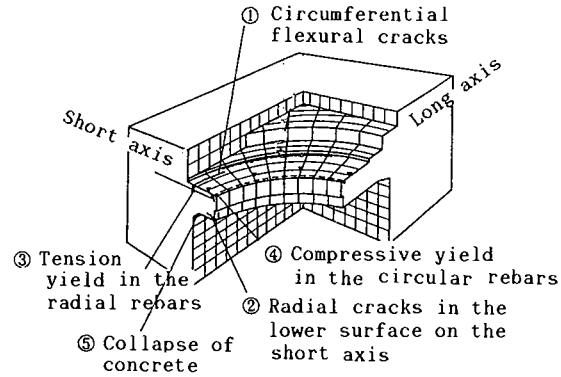

Fig.14 Failure process

(2) Vertical Displacement at the Loading Points

Fig. 15 shows the load-vertical displacement relationship in 90 degree (and 270 degree) directions. Fig. 16 shows the circumferential load-vertical displacement relationship in each direction, expressed on an envelope curve. The envelope curves for each direction are all similar each other. As flexural cracks occurred at the beginning, there was slightly loss of rigidity. Furthermore, there was no development of displacement or load drop with rebar yield, and the hysteresis curve remained extremely stable to the end of the experiment. Overall, even after yield in the radial rebars, it is suggested that the effects of the plate have prevented a sudden drop in stiffness. As shown in Fig. 17, there was a tendency for vertical displacement, which was slightly more prominent along the long axis than on the short axis.

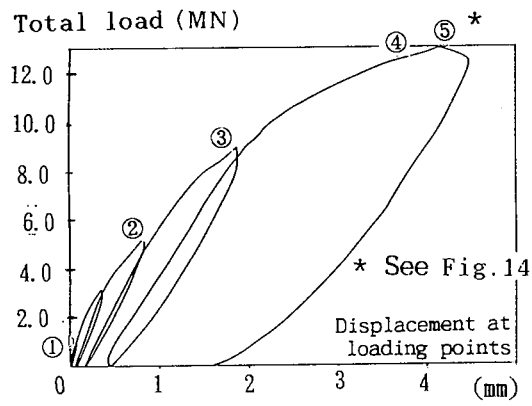

Fig.15 Load-displacement relationship in 90(270) degrees

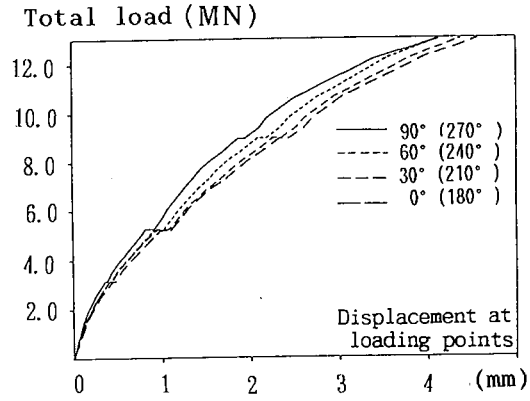

Fig.16 Load-displacement relationship

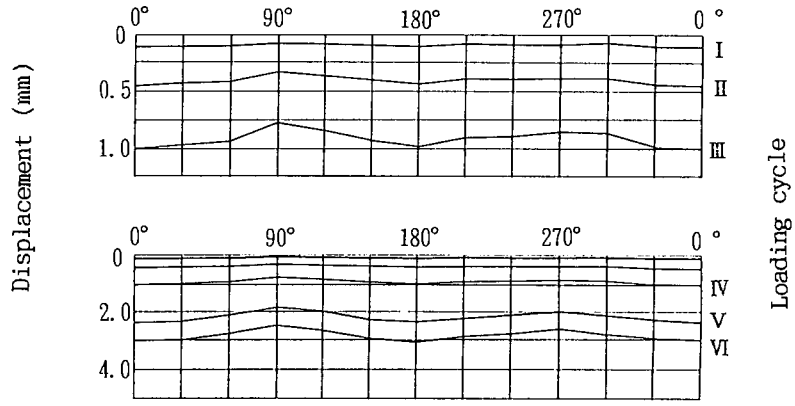

Fig.17 Distribution of vertical displacement (peak load of each cycle)

(3) Radial Rebar Strain

Fig. 18 shows the load-strain relationship in each direction for radial rebars, expressed on an envelope curve. Upper rebars showed tension strain, while lower rebars showed compressive strain. In the upper radial rebars, the shorter the span, the faster the strain progressed, while strain progressed more slowly in the lower radial rebars. With the total load ranging from 2.0 MN to 4.0 MN, there was a temporary increase in upper radial rebar strain, because of the development of flexural cracks in the circumferential direction on the upper surface of the slab. This was slightly more prominent along the long axis than on the short axis. As for the lower rebars, the occurrence of initial cracks produced little change in the curve. The compressive strain in the lower rebars on 90 (270) degree directions was relatively small compared with that in other directions. Furthermore, compressive strain was reduced when total load approached 8.0 MN, in 90 (270) degree directions for the overall model. It is also occurred in the partial model P1 and P3 specimens, and suggesting that a truss type shear transfer mechanism was formed.

(4) Circular Rebar Strain

An envelope curve for the load-strain relationship in each direction for the circular rebars at the loading points is shown in Fig. 19. Looking at the model as a whole, the upper rebars registered compressive strain resulting in compressive rings, while the lower rebars showed tension strain producing tension rings. It is suggested that the upper compressive stress ring have restrained vertical displacement of the slab. The strain in the upper rebars was not influenced by cracks or yield rebars, and increased smoothly as the load was increased. Strain along the 90 (270) degree directions was smaller than strain shown in other directions, up until the load ratio changed. Strain in the lower circular rebars in the 90 (270) degree and 60 (240) degree directions increased suddenly with the development of initial cracks on the upper slab.

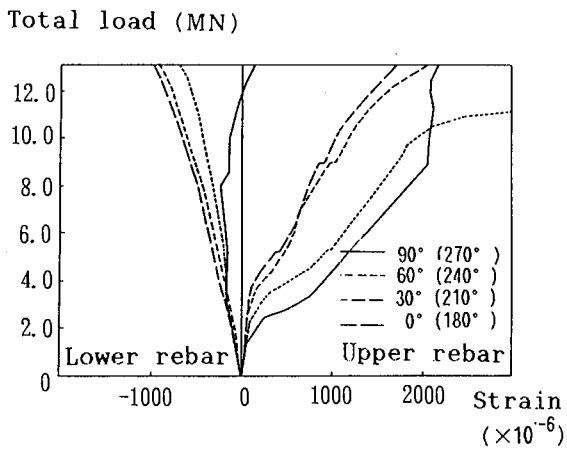

Fig.18 Load-radial rebar strain relationship

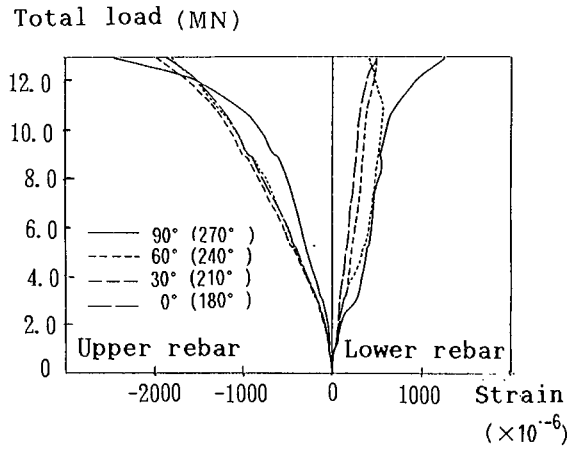

Fig.19 Load-circular rebar strain relationship

(5) Shear Rebar Strain

An envelope curve for the load-strain relationship for shear rebars is shown in Fig. 20. Compressive strain appeared in the 90 (270) degree direction at the beginning, just as in the partial model P1 specimen. This shifted to tension strain with increase in the load. Compressive strain in other directions was close to zero at low load levels, but also shifted to tension strain with load increase. This tendency to shift toward tension strain with load increase registered higher values, with the largest shear crack strength found in the short axis. In this experiment there was no evidence of yield in shear rebars.

(6) Final Condition of the Specimen

Fig. 21 shows the cracks on the upper surface of the slab at the time of maximum load. While no cracks were evident in the upper slab under live load, after an increase of load by a factor of 1.4, circular cracks did develop along the short axis. Circular cracks spread with the increase of load, and finally covered the surface of the slab at a level of 9 times the amount of the live load. Altogether, there were 3 concentric cracks.

When upper radial rebar yield occurred, radial cracks occurred on the lower surface of the slab along the short axis in the area of the opening, and the number of cracks increased with the increase in load. Under a force of 10.4 MN to 12.7 MN, compressive failure occurred at the haunch.

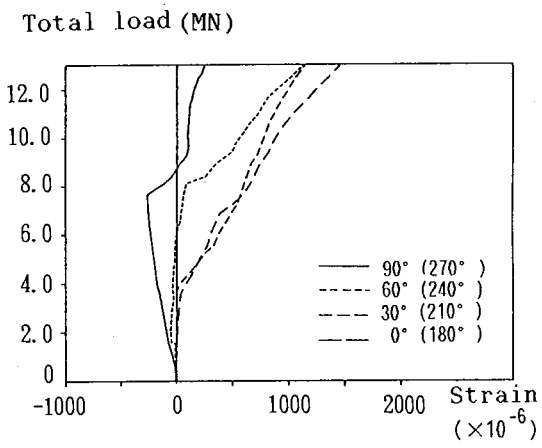

Fig.20 Load-shear rebar strain relationship in 90(270) degrees

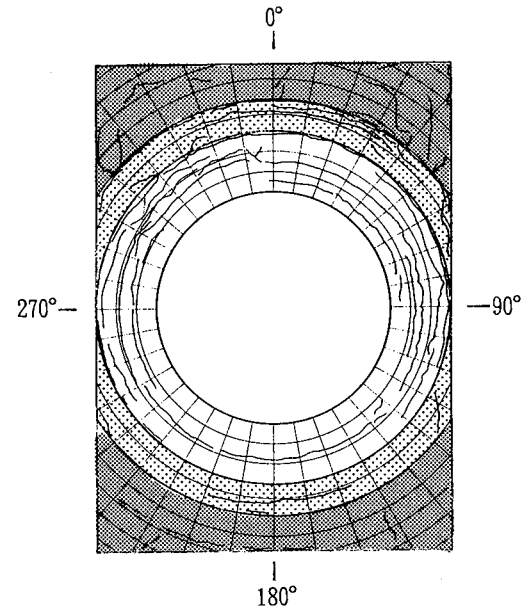

Fig.21 Final condition of the overall model specimen(upper surface)

4.3. Overall Specimen Failure Mode

Test results made clear that the ultimate strength of the support slab was reached at a value of 12.5 times that of the weight of the reactor. It is also clear that the failure mode of the support slab was of the flexural failure type.

5. Conclusions

Focussing on the reactor support slab used in the demonstration plant of the advanced thermal reactor (ATR), this research involved static loading tests and non-linear FEA. The results showed that the failure mode of the reactor core support slab is of the flexural failure type, and the support slab possessed adequate ultimate strength. Accordingly, the bending strength of the support slab is approximately and conservatively estimated as the sum of the strength of the short span cantilever beams. Furthermore, the failure process of the support slab is simulated based on the non-linear FEA , using layered shell elements and it is confirmed that the analytical code is applicable to the design for the reactor support slab of an ATR. Therefore, the structural safety of the support slab for a reactor core with respect to out-of-plane shear force is confirmed.

Acknowledgments:

We would like to express our sincere appreciation to Professor H. Aoyama of Tokyo University, and Professor M. Hirosawa of Kogakuin University, for their invaluable assistance at all phases of this study.

References:

"Standard for Structural Calculation of Reinforced Concrete Structures," 1990, Architectural Institute of Japan (AIJ).